Chemical and Dynamical Impacts of Stratospheric Sudden Warmings on Arctic Ozone Variability

S.E. Strahan[1,2], A.R. Douglass[2], and S.D. Steenrod[1,2]

[1]Universities Space Research Association, Columbia, MD

[2]NASA Goddard Space Flight Center, Atmospheric Chemistry and Dynamics Laboratory, Greenbelt, MD

Main points

Arctic column ozone depletion depends on the number of cold days

Winters with a sudden warming have less than half the depletion of years without one

Dynamics plays a larger role than chemistry in Arctic ozone variability

Abstract. We use the Global Modeling Initiative (GMI) chemistry and transport model with Modern-Era Retrospective Analysis for Research and Applications (MERRA) meteorological fields to quantify heterogeneous chemical ozone loss in Arctic winters 2005-2015. Comparisons to Aura Microwave Limb Sounder N_2O and O_3 observations show the GMI simulation credibly represents the transport processes and net heterogeneous chemical loss necessary to simulate Arctic ozone. We find that the maximum seasonal ozone depletion varies linearly with the number of cold days and with wave driving (eddy heat flux) calculated from MERRA fields. We use this relationship and MERRA temperatures to estimate seasonal ozone loss from 1993-2004 when inorganic chlorine levels were in the same range as during the Aura period. Using these loss estimates and the observed March mean 63-90^{o}N column O_3, we quantify the sensitivity of the ozone dynamical resupply to wave driving, separating it from the sensitivity of ozone depletion to wave driving. The results show that about 2/3 of the deviation of the observed March Arctic O_3 from an assumed climatological mean is due to variations in O_3 resupply and 1/3 is due to depletion. Winters with a stratospheric sudden warming (SSW) before mid-February have about 1/3 the depletion of winters without one and export less depletion to the midlatitudes. However, a larger effect on the spring midlatitude ozone comes from dynamical differences between warm and cold Arctic winters, which can mask or add to the impact of exported depletion.

1. Introduction

The global distribution of stratospheric ozone outside the tropical production region is largely controlled by the circulation. Transport from the tropical middle stratosphere (~5-20 hPa) increases ozone at the poles during winter and spring. In the northern hemisphere, large interannual variability in the strength of planetary waves driving the winter circulation leads to large variability in Arctic spring column ozone [Randel et al., 2002; Weber et al., 2011]. Arctic spring ozone levels began to decline in the 1980s as levels of anthropogenic ozone depleting substances (ODSs) increased, leading to additional Arctic column ozone variability. ODSs are chlorine and bromine-containing compounds with long atmospheric lifetimes that are the sources of most stratospheric reactive halogen species. Ozone depletion each year varies greatly because stratospheric temperature variations affect polar stratospheric cloud (PSC) formation and the subsequent production of reactive halogens. In both hemispheres, winter wave driving controls polar vortex spring temperatures [Newman et al., 2001] and poleward transport of ozone [Randel et al., 2002; Weber et al., 2003]. October (Antarctic) and March (Arctic) mean column O_3 (63-90^o) determined from satellite observations are often used as indicators of ozone depletion, e.g., WMO [2014] and prior assessments. Because the Antarctic vortex frequently covers the 63-90^{o}S area and winter ozone resupply is weak and less variable than the Arctic [Weber et al., 2003], the severity of depletion may be qualitatively assessed by the difference between the observed October 63-90^{o}S mean and the estimated pre-1980 climatological value. Determining the degree of anthropogenic ozone depletion based on Arctic March column O_3 variability, however, is problematic because the Arctic vortex is typically smaller than the Antarctic vortex and the 63-90^{o}N area usually includes midlatitude air.In addition, stronger and more variable wave driving in the northern hemisphere leads to large interannual variability in both dynamical resupply and chemical depletion of ozone (e.g., Tegtmeier et al., [2008]).

Explaining Arctic spring ozone variability is a prerequisite for detecting changes in polar ozone. ODS levels in the stratosphere have been declining since the late 1990s, but the detection and attribution of an increase in polar ozone due to declining ODSs requires a quantitative separation of chemical depletion from variable seasonal O_3 transport (i.e., dynamical resupply). Some studies have focused on calculating the chemical loss component of spring ozone variability. Ozone losses in the Arctic lower stratosphere have been calculated with sonde data [Rex et al., 2002, and references therein] and with satellite data [Manney et al., 2003; Livesey et al., 2015a] using the 'Match' method that combines observations with reanalysis meteorology in a trajectory model. The trajectory model is used to identify

air parcels whose trajectories are inside the vortex. Ozone loss is then calculated as the difference between ozone measurements in the same vortex air parcel on different dates. The accuracy of this method strongly depends on vortex isolation. Rex et al. [2004] calculated vortex-averaged lower stratospheric losses ranging from 20-88 DU from 1992-2002. Livesey et al. [2015a], using Aura MLS O_3 data from 2004-2011, calculated losses ranging from 22-116 DU. Other studies have computed lower stratospheric partial column O_3 losses using the tracer-tracer method [Mueller et al., 2001; Tilmes et al., 2003], which assumes a constant relationship inside the vortex between O_3 and a long-lived trace gas, often N_2O, throughout winter. Any mixing across the vortex edge during winter changes the relationship and leads to an underestimate of ozone loss [Mueller et al., 2005], thus this method is best suited for winters with a strongly isolated polar vortex. Livesey et al. [2015a] compared published ozone loss estimates for the winter 2004/5 and noted that the wide range of reported losses indicates the challenge of quantifying ozone depletion in a way that properly accounts for transport processes.

Chemistry and transport models (CTMs) integrated with reanalysis meteorology provide an alternative method for assessing ozone depletion by explicitly calculating both the chemical depletion and the transport contributions to Arctic spring ozone. Using CTM simulations of 1991-1998 with and without the effects of chlorine activation on PSCs, Chipperfield and Jones [1999] calculated a 7-yr average column O_3 loss of 38 DU and a mean dynamical resupply of 80 DU. They concluded that the variability of vortex ozone depletion was much smaller than the observed column O_3 variability 63-90^{o}N. However, the results of CTM calculations using reanalyses from more than a decade ago are uncertain because their meteorological fields have excessive mixing and a poor transport circulation due to the assimilation process [Schoeberl et al., 2003; Tan et al., 2004]. Tegtmeier et al. [2008] calculated the contributions of depletion and dynamics to spring column O_3 for 1992-2004 using the Match method for the chemical losses and a reanalysis-derived diabatic descent rate to estimate the dynamical increases in lower stratospheric O_3. They estimated that the O_3 increase due to vortex-averaged diabatic descent varied from 60-140 DU, while chemical depletion varied from 10-100 DU, concluding that the two effects were anti-correlated and contributed equally to Arctic column O_3 variability. Their analysis assumed that the vortex remained isolated through March.

It is rare for the Arctic vortex to remain strongly isolated throughout winter. Wave-driven mixing across the vortex edge adds uncertainty to the Match and tracer-tracer methods. Using a 40-yr meteorological reanalysis, Charlton and Polvani [2007] showed that 6 out of 10 winters experienced a major mid-winter stratospheric sudden warming (SSW), defined as a weakening or reversal of the zonal mean zonal wind

at 60°N 10 hPa, accompanied by rapid polar warming. SSWs weaken the vortex circulation and allow poleward transport of ozone rich midlatitude air. SSWs also increase temperatures in the lower stratosphere, halting chlorine activation and ozone depletion. The changes in vortex isolation and temperature caused by SSWs clearly affect ozone depletion, but no quantitative relationship has been demonstrated. Manney et al. [2015] report large variability in ozone loss in years with comparable SSWs (2003 and 2010). Kuttipurrath and Nikulin [2012] examined Arctic O_3 depletion from 1994-2010 and concluded that loss was qualitatively proportional to the intensity and timing of SSWs and the volume of polar stratospheric clouds (PSCs), noting that ozone loss in winters with an early season SSW was less than in winters with a late season warming. This suggests a role for SSWs in modulating the impact of polar depletion on midlatitude spring ozone.

In this paper, we use the Global Modeling Initiative (GMI) chemistry and transport model with Modern-Era Retrospective Analysis for Research and Applications (MERRA) meteorological fields to quantify the heterogeneous chemical ozone loss in the Arctic for the winters 2005-2015. The methods used here provide a reliable, quantitative approach to separating the chemical and transport contributions to Arctic ozone changes because of the simulation's realistic representation of vortex descent and isolation as well as meridional transport and chemical processes. The methods and model evaluation are described in Section 2 and in the Appendix. In Section 3 we calculate Arctic O_3 depletion for 11 winters and quantify the relationship between depletion, vortex temperature, and eddy heat flux. We show that winters with a SSW have significantly diminished ozone depletion. Section 4 uses the results of Section 3 to estimate Arctic spring ozone loss in years 1993-2004, prior to the launch of the Aura satellite (July 2004). Using model results and total column O_3 observations, we show distinct relationships between wave driving and ozone depletion, and between wave driving and ozone resupply. Section 5 shows how depletion and O_3 transport have different spatial impacts on midlatitude ozone and surface UV in spring, depending on the occurrence of a midwinter stratospheric sudden warming. The results of this study are summarized in Section 6.

2. Observations, the GMI Model, and Methods

This study uses Aura Microwave Limb Sounder (MLS) v4.2 Level 2 profile measurements of O_3 between October 2004 and May 2015 (Livesey et al., 2015b); they are reported on a vertical resolution grid with 12 pressures per decade. We calculate MLS ozone columns using levels 268-0.46 hPa and refer to them as the stratospheric column; the reported 2σ column accuracy is 4%. The 268 hPa level is generally near the tropopause inside the vortex. MLS v3.3 N_2O and temperature data from October 2004 to May 2013

122 are used for CTM transport evaluation in the lower stratosphere (46-100 hPa), where the N_2O 2σ
123 accuracy is 14% (Livesey et al., 2011). The primary MLS band used to retrieve N_2O failed in June 2013.
124 Ongoing retrievals using Band 3 (190 GHz) are scientifically useful from 68-0.46 hPa but are high biased
125 and noisy at 68 hPa. The transport evaluation is therefore restricted to dates before the primary band
126 failure. We also use satellite observations of March total column O_3 from the NASA GSFC Ozone and Air
127 Quality website (http://ozoneaq.gsfc.nasa.gov/). The column O_3 data sets we use cover the period 1979
128 to the present nearly continuously and consist of measurements from several different instruments,
129 from the Total Ozone Mapping Spectrometer (TOMS) on Nimbus-7 to the Ozone Measuring Instrument
130 (OMI) on the NASA Aura satellite.

131 The GMI CTM was integrated from January 1, 2004-May 31, 2015 using MERRA reanalysis
132 meteorological fields (Rienecker et al., 2011) with 1^{o}x1.25^{o} horizontal resolution and 72 vertical levels
133 having ~1 km resolution between 300-10 hPa. Details of the GMI CTM and this simulation are found in
134 Strahan et al. [2013] and references therein. For the period of the simulation, all organic halogen
135 species and other long-lived species are forced by appropriately changing mixing ratios at the surface. In
136 addition, a second GMI simulation ('No Het') was integrated with the rates for heterogeneous reactions
137 involving chlorine and bromine set to zero for the months October to May. This eliminates halogen
138 activation by all PSC particle types. Both simulations have the same transport because they are
139 integrated with the same MERRA meteorology and there is no feedback between simulated O_3 and
140 dynamics. The 'No Het' simulation is initialized on October 1 each year with conditions from the full
141 chemistry simulation. The difference in O_3 fields between the 'No Het' and the full chemistry simulation
142 measures the heterogeneous chemical loss independent of dynamical changes in O_3.

143 A CTM experiment requires the realistic representation of ozone loss processes and transport over the
144 course of winter to accurately calculate polar O_3 change. A simulation must, for example, closely
145 reproduce long-lived tracer observations inside the vortex to demonstrate that isolation and descent are
146 well-represented. This is critical for simulating the dynamical supply of ozone. Strahan et al. [2013]
147 demonstrated the transport and chemistry credibility of this GMI simulation by showing close
148 agreement between this simulation and MLS N_2O, O_3, and ClO profiles inside the Arctic vortex during the
149 winter of 2011. In the Appendix we demonstrate the fidelity of this simulation throughout the Aura
150 period using comparisons with observations in 4 winters with widely varying Arctic vortex strength. The
151 comparisons to MLS N_2O in Figure A1 verify that before the final warming, the simulation produces
152 realistic transport in the Arctic lower stratosphere whether the vortex is strong or weak. The lower

153 panels of Fig. A1 show that the simulated column O_3 changes closely track the MLS O_3 changes.
154 Together, the N_2O and O_3 comparisons demonstrate the credibility of this simulation's net
155 heterogeneous chemical loss and its high latitude circulation and mixing.

156 The simulation is limited to the period of the Aura satellite, 2004–2015, for reasons related to MERRA
157 transport fidelity prior to Aura. Aura MLS observations provide the first global daily profile datasets of
158 ozone and a long-lived source gas (N_2O). Abalos et al. [2015] compared the Brewer Dobson Circulation
159 (BDC) obtained from three modern reanalyses including MERRA, and showed substantial differences in
160 the tropical upwelling (up to 40%). Although they do not evaluate the BDC in polar regions or the
161 representation of the polar vortex and its isolation, such a large level of uncertainty in the BDC indicates
162 the necessity of a dataset like MLS for evaluation. Comparisons of MERRA-driven simulations in the
163 1990s with datasets from the Upper Atmosphere Research Satellite (UARS) instruments such as the
164 Cryogenic Limb Array Etalon Spectrometer (CLAES) and the HALogen Occultation Experiment (HALOE)
165 reveal issues with the subtropical gradients in long-lived tracers and a poor representation of the effects
166 of the quasi-biennial oscillation. Our evaluation of MERRA's circulation prior to Aura suggests caution
167 and comprehensive evaluation is not possible. Note that we use v'T' computed from MERRA for 1993–
168 2004; this product of deviation from the mean is much more certain than the residual circulation fields,
169 v* and w*.

170 The constituent analyses use the equivalent latitude/potential temperature coordinate system
171 calculated from daily MERRA potential vorticity (PV) and temperature fields. Potential vorticity is a good
172 tracer of atmospheric motions because it is conserved on a timescale of weeks in the lower
173 stratosphere. Equivalent latitude is calculated by mapping daily PV fields (on potential temperature
174 surfaces) onto equal areas centered on the pole; the same mapping is then applied to a trace gas field,
175 creating a vortex-centered coordinate [Nash et al., 1996]. This mapping allows the definition of a
176 dynamical boundary between the polar vortex and midlatitude air masses, advantageous for studies of
177 polar processes such as ozone depletion [Manney et al., 2003, Mueller et al., 2008]. We use an Arctic
178 cap average, defined as the area-weighted mean over 63-90^{o}N equivalent latitude (EqL), to analyze polar
179 processes. MLS and GMI stratospheric ozone columns are calculated using the same pressure range,
180 268-0.46 hPa. MERRA zonal wind and temperature are also used to identify minor and major SSWs.
181 MERRA minimum temperatures in the Arctic winter lower stratosphere have been shown to agree
182 within 1 K with ERA-Interim temperatures after 1997 and to within 1.4 K before that [Lawrence et al.,
183 2015]. The dynamical analyses use the daily 100 hPa zonal mean eddy heat flux, v'T', averaged from 45-

75°N over the preceding 45 days; it is available from the NASA Goddard data services website (http://acdb-ext.gsfc.nasa.gov/Data_services/met/ann_data.html). The 45-day averaging comes from the radiative damping timescale in the lower stratosphere, as used in Newman et al. [2001].

3. Dynamical Control of Ozone Depletion, 2005-2015

Temperature and ODS levels are the primary factors controlling polar ozone depletion [Newman et al., 2004]. Levels of stratospheric inorganic chlorine (Cl_y) have declined roughly 8% between 2005 and 2015 due to declining ODS levels, but Cl_y in the winter polar lower stratosphere remains above 2.5 ppb, a level 50% greater than 1980 values [Strahan et al., 2014]. Because year-to-year variations in Cl_y levels are small, temperature variations exert primary control over interannual variations in polar ozone depletion [Newman et al., 2006]. This analysis investigates the influence of dynamics on ozone depletion through vortex stability and temperature.

3.1 Quantifying Arctic Ozone Loss

In this section we calculate the column O_3 change due to heterogeneous chemical loss in all Arctic winters 2005-2015 using the difference between the GMI full chemistry and 'No Het' simulations. The column O_3 differences between these simulations provide a daily look at ozone depletion throughout the Arctic that cannot be obtained by observations alone. Figure 1 shows the maximum seasonal depletion in 4 years with widely varying dynamical conditions. The top panels show years where a SSW caused a split (2013) or displaced (2010) vortex, leading to high temperatures that ended ozone depletion by midwinter. The lower panels show two cold, weakly disturbed years with a mid-March (2005) and a mid-April (2008) final warming. Maximum local losses in these two years without a SSW were greater than 60 DU while the disturbed winters had a maximum loss near 30 DU. The greatest losses of this decade were shown in Strahan et al. [2013], when local losses exceeded 100 DU in late March 2011.

The equivalent latitude coordinate (EqL) accounts for variations in vortex size and shape, allowing the magnitude of depletion to be easily compared each year. Figure 2 shows 11 years of daily ozone depletion mapped onto equivalent latitude using MERRA potential vorticity on the 450 K isentropic surface. The 450 K surface is near the midpoint of the altitude range of ozone depletion (~350-540 K, or 150-30 hPa). Figure 2 shows that O_3 depletion varies greatly over the 11 years, with maximum losses each year ranging from 21 to 93 DU. The region of steep O_3 loss gradients is generally co-located with the vortex edge. These gradients are found at the lowest latitudes in 2005 and 2014, indicating a very large vortex.

The patterns in Figure 2 fall into two groups based on the timing and magnitude of the loss. Five years (2005, 2007, 2008, 2011, and 2014) maintain losses of more than 40 DU for at least 6 weeks, with a maximum loss of >50 DU occurring in March. The other 6 years have a maximum loss less than 40 DU, and except for 2015, the maximum occurs in January or February. In all years the maximum loss occurs north of 80^{o} EqL. The years with high losses also have higher losses at lower latitudes. The high loss group has losses of 25-50 DU at 70^{o} EqL, while the losses there never exceed 25 DU in the low loss group. The high loss group also stands out in April because losses >5 DU appear south of 50^{o} EqL.

Figure 3 shows the daily Arctic cap mean, defined as the area-weighted mean depletion between 63-90^{o} equivalent latitude, to summarize the year-to-year depletion variations shown in Figure 2. This quantity, used in previous studies (e.g., Mueller et al, [2008]; WMO [2014]), captures essentially all of the ozone loss that occurred inside the vortex shown in Fig. 2. There are many similarities each year in the evolution of Arctic cap loss. Depletion in December is small: ≤1 DU before the 10th and still less than 4 DU in most years by the end of the month. Very low temperatures that persisted throughout a deep layer of the lower stratosphere in December 2012 led to a higher early season loss rate in 2013 than other years [Manney et al. 2015]. By the end of January, all years have 11-18 DU loss, except 2015, which had warm early winter temperatures that delayed the onset of depletion. But in February there are large year-to-year variations in losses and by March 1, the losses have separated into two groups: 6 years with maximum losses from 12-22 DU (dashed lines), and 5 years with losses from 30-52 DU (solid). The mean loss in the high loss group (41 DU) is nearly three times greater than the mean of the low loss group (16 DU).

3.2 Ozone loss and Heat Flux

It is well-known that polar ozone depletion is controlled through the temperature-dependence of PSC particle formation and the subsequent production of active forms of chlorine and bromine [Kawa et al., 1997]. Wohltmann et al. [2013] showed there is a strong linear relationship between chlorine activation and column O_3 loss, and that modelled loss was insensitive to the details of the chlorine activation (i.e., particle type). We look for a relationship between the maximum Arctic cap ozone loss shown in Figure 3 and the number days with lower stratospheric vortex temperatures below the threshold for particle formation. We use MERRA temperatures and the Hanson and Mauersberger [1988] kinetics constants to calculate the temperature thresholds for particle formation on 5 MERRA pressure levels from 150-30 hPa. We count the number of days each season with below-threshold temperature anywhere inside the vortex on at least 2 pressure levels. The area of below-threshold temperatures is not considered, and

246 only days after December 15th are counted because there is negligible loss before. Figure 4a shows a
247 highly correlated (0.97) approximately linear relationship between the maximum seasonal Arctic cap
248 column O_3 depletion and the number of days when vortex temperatures were at or below particle
249 formation temperatures on at least 2 pressure levels. A similar relationship, but with greater scatter, is
250 found when we require below-threshold temperatures on only 1 level. Similar results would likely be
251 obtained using the ERA-Interim reanalysis. Lawrence et al. [2015] showed that the number of days each
252 Arctic winter with temperatures below the PSC activation threshold in MERRA agreed to within a few
253 days to the number found in ERA-Interim from the 1980s to the present.

254 Figure 4a shows that the severity of seasonal Arctic ozone loss can be estimated to within ± 6 DU based
255 on the number of cold days inside the vortex. The loss rate is ~0.5 DU loss/cold day over a range of 12-
256 52 DU loss for 2005-2015, for current high Cl_y conditions in the polar lower stratosphere (mean age ~5
257 yrs). Over the past decade Antarctic Cl_y has been estimated to vary between 2.55-2.95 ppb [Strahan et
258 al., 2014]. We expect Arctic Cl_y values to be similar because the mean age and the age spectrum of the
259 Arctic lower stratosphere are similar to the Antarctic [Li et al., 2012]. As ODS levels slowly decline, the
260 slope of this line will flatten [Weber et al. 2011]. The Cl_y decline rate of less than 1%/yr is too slow to
261 have a discernable effect on the fitted slope, which has 1σ uncertainty of 10%.

262 This result is similar to the relationship found by Rex et al. [2004] between the Arctic column ozone
263 depletion and the volume of air with seasonally-averaged (December-March) temperatures below PSC
264 thresholds (V_{psc}). Our result suggests that the key factor to loss is the *duration* of low temperatures
265 rather than their *volume*. Duration is implicitly a factor in their result because they used a seasonal
266 average of vortex temperatures, however, because V_{psc} depends on the area of low temperatures while
267 our metric does not, a given V_{psc} does not uniquely correspond to the number of cold days; the
268 correlation of V_{psc} and cold days during the Aura period is 0.74. We find a correlation of 0.97 between O_3
269 loss and the number of cold days (Fig. 4a), and a significant but lower correlation between O_3 loss and
270 V_{psc}, 0.85. Our results for the seasonal maximum loss averaged over 63-90^{o}N EqL are roughly half the
271 loss estimates reported for 2005-2011 by Livesey et al. [2015a] using MLS O_3 measurements and the
272 Match method. They report that ozone loss estimates are sensitive to the value of potential vorticity
273 chosen to define the vortex edge by affecting the area over which losses are averaged. For this reason,
274 the conservative potential vorticity criteria they apply to their matches are likely to result in larger loss
275 estimates than ours because they average over higher equivalent latitudes where losses are greater.
276 They note that when the vortex is disturbed, meridional transport and mixing will lead greater error in

their estimates. Our method properly accounts for those contributions to Arctic O_3 regardless of the degree of disturbance.

Newman et al. [2001] demonstrated that the strength and temperature of the polar lower stratospheric vortex are controlled by planetary wave driving, finding a relationship between the mean midwinter 100 hPa eddy heat flux from 45-75°N (v'T') and the March 50 hPa temperature 60-90°N. The eddy heat flux is proportional to the vertical component of the Eliassen-Palm flux, which we use here as a measure of planetary wave driving. Figures 4b and 4c show that the number of cold days and the maximum seasonal heterogeneous chemical loss, both driven by temperature, are strongly correlated with the 100 hPa heat flux averaged over the period where most depletion occurs (mid-December through February). Figure 4b shows that years with a larger numbers of cold days are associated with lower heat fluxes, consistent with the results of Newman et al. [2001] that showed weak wave driving leads to a stable, long-lived vortex. 2011 had the greatest number of days with temperatures below PSC thresholds and is tied with 2005 for the weakest wave driving (Dec 15-Feb 28 average) of the Aura period.

3.3 The Impact of Stratospheric Sudden Warmings on O_3 Depletion

Six of 11 recent winters had much less seasonal loss, fewer cold days, and stronger wave driving than the other years. Strong wave driving can lead to a stratospheric sudden warming, defined as the reversal of the zonal mean zonal wind at 10 hPa and 60°N, accompanied by a rapid reversal of the poleward zonal mean temperature gradient [Andrews et al., 1987]. The warming is minor when the temperature gradient reverses but the zonal wind does not. The warming is final if the return to westerly zonal winds lasts fewer than 10 consecutive days [Charlton and Polvani, [2007]. We use these criteria and MERRA wind fields to assess Arctic winters 2005-2015. The years 2006, 2009, and 2013 are at the low loss end of Figure 4a (<15 DU) and all experienced a January major SSW with a wind reversal persisting at least 3 weeks. The years 2010 and 2012 had minor warmings that did not quite attain the major SSW definition, but had westerlies that dropped from ~40 m/s to 10 m/s or less for a month or more. The minor warming in early January 2015 had 10 hPa 60°N winds that dropped from 40 to ~20 m/s for more than a month. These six years with SSWs averaged 37 days sufficiently cold for Cl activation and had seasonal Arctic cap losses of 12-22 DU.

None of the 5 high loss years (2005, 2007, 2008, 2011, and 2014) had a major or minor warming before mid-February. The 60°N 10 hPa winds in these 5 years remained high (>20 m/s) from December through mid-February or later and had temperatures that were usually near or below average. These conditions led to a vortex that was relatively undisturbed until late winter, allowing Cl activation to persist roughly

6 weeks longer than the disturbed winters. These years experienced Arctic cap maximum losses of 30-52 DU.

We use the occurrence of a stratospheric sudden warming, major or minor, before late winter to divide the years 2005-2015 into two groups. Figure 5 shows the mean differences in the magnitude, timing, and midlatitude impact of Arctic ozone depletion in winters with a SSW (referred to as warm or disturbed) and those with a more stable vortex (referred to as cold or stable). The means are calculated from the results in Figure 2. In disturbed years, a mean maximum loss of 22 DU occurs north of 84^{o} equivalent latitude in mid-February. The impact on the midlatitudes in spring is small, on average less than 5 DU south of 50^{o}. By early May there are no losses greater than 10 DU at any latitude. In contrast, years with a stable vortex have an average maximum loss nearly 3 times greater, 62 DU, that occurs about a month later than the disturbed years. The larger magnitude, larger areal extent, and late March timing of the maximum loss can result in a larger impact on lower latitudes in spring when surface UV levels are rapidly increasing. Ozone depletion at polar latitudes in April is also substantially greater in cold years (~15-57 DU) compared to disturbed years (10-18 DU). By May all losses have diminished but cold year losses remain about twice the size of disturbed year losses.

4. March Arctic Ozone Variability, 1993-2015

Figure 3.4 in Chapter 3 of the WMO Ozone Assessment [, 2014] shows large year-to-year variability in Arctic March mean total column O_3 in the past 30 years, with some values more than 100 DU below the figure's implied climatological mean value of 455 DU. We calculate the March average loss over the geographic (*i.e.,* not equivalent latitude) Arctic cap for 2005-2015; this is the same space and time averaging used in the WMO Assessment. This area-averaged loss also has a linear relationship with the number of cold days, and we use this relationship and meteorological data to estimate losses for 1993-2004. By adding the estimated loss to observed March O_3 from 1993-2015, we determine a relationship between wave driving and March O_3 in the absence of halogen catalyzed ozone loss. The results presented here quantitatively explain the sources of observed Arctic March O_3 variability. GMI-MERRA simulations cannot be used to quantify ozone depletion during the 1990s because of known uncertainties in the MERRA transport circulation described in Section 2 and the lack of satellite measurements needed for a comprehensive evaluation of polar ozone transport.

4.1 Estimation of March Arctic Ozone Depletion before Aura

To understand the variability caused by depletion in the multi-decadal March Arctic O_3 record, we calculate the March monthly mean column O_3 depletion from the GMI simulations, 2005-2015, averaged

over 63-90°N geographic latitude as in WMO [Dameris and Godin-Beekmann, 2014]. Figure 6a shows a highly correlated relationship, similar to Fig. 4a, between the mean March 63-90°N depletion and number of cold days. We use the slope of the line in Fig. 6a to estimate the March depletion in the years prior to Aura. The number of cold days inside the vortex each year from 1993-2004 was determined from MERRA temperatures and potential vorticity (to identify the vortex), using the same criteria described in Section 3. Using the slope in Fig. 6a and the number of cold days each year, we estimate the March average 63-90°N ozone depletion for years 1993-2004. This is shown in Figure 6b along with the loss values for 2005-2015 (from Fig. 6a). We exclude years prior to 1993 from this analysis because polar lower stratospheric Cl_y is estimated to be lower than 2004-2015 levels [Newman et al., 2007] and the relationship between depletion and cold days (Fig. 6a) would have a different slope. None of the years 1993-2004 had more cold days than the coldest Aura year (2011) and 3 had fewer cold days than the warmest Aura year (2013). The estimated losses from 1993-2015 range from 1-39 DU, with an average of 18 DU. Based on the deviations from the linear fit shown in Fig. 6a, the 2σ uncertainty of the loss estimates is 5.5 DU.

Figure 7 shows the time series of observed Arctic March O_3 from TOMS and OMI instruments from 1979-2015. The red dashed line is the March mean heterogeneous loss (from Fig. 6b) added to the observed March column O_3; it is referred to as 'No Het Loss' O_3. The losses are shaded in blue. The yellow shading represents the difference between the estimated March 'No Het Loss' O_3 and the 455 DU 'climatological mean' value implied by WMO Figure 3.4. This figure reveals that depletion usually accounts for less than half the difference between 455 DU and the observations. The average 'No Het Loss' March O_3 ranges from 375 to 464 DU, averaging more than 30 DU below the implied climatological mean. As a result, the observed March O_3 in the WMO figure gives the impression of much greater depletion than actually occurs. By calculating the percentage of March ozone loss with respect to the 'No Het Loss' O_3 values determined here (rather than 455 DU), we find the largest depletion of the 1993-2015 period is 10% in 2011; the average is 4.4%. Even with a 5.5 DU 2σ loss uncertainty, depletion (blue shading) usually accounts for less than half of the observed difference from 455 DU (blue and yellow together). This is shown as the depletion fraction at the bottom of the figure.

4.2 Sensitivities of O_3 Resupply and O_3 Depletion to Wave Driving

Quantitatively separating wave driving's effect on ozone resupply from its effect on ozone depletion is challenging because polar ozone is affected by each process in the same sense: stronger wave driving is associated with increased ozone (increased resupply and reduced loss) whereas weaker wave driving is

associated with decreased ozone (reduced resupply and increased loss). Total column O_3 observations from 1993-2015 and the 'No Het Loss' O_3 time series provide a way to separate polar ozone sensitivities. We use the 45-75^{o}N mean 100 hPa heat flux averaged from December through March as a measure of the strength of the wave driving that affects March ozone. Figure 8a shows the relationship between wave driving and March 'No Het Loss' O_3, which reflects the sensitivity of resupply to dynamics in the absence of depletion. The relationship is highly correlated (0.73) and the slope of the best fit line is 11.7 ± 2.0 DU/Kms^{-1}. Figure 8b shows the relationship of wave driving and the March O_3 observations, which indicates the combined sensitivity of resupply and depletion to dynamics. The correlation of these points is 0.79 and the slope is 16.4 ± 2.2 DU/Kms^{-1}. Fall wave driving is small compared to winter and its inclusion in the analysis period does not increase the correlation. The range and mean of the heat fluxes from 1993-2004 (open symbols) are approximately the same as the range and mean of the Aura period (solid symbols), indicating no trend in wave driving during this 23 year period that might affect observed Arctic O_3 variability.

The difference of the slopes in Fig. 8b, 4.7 ± 3.0 DU/Kms^{-1}, represents the sensitivity of O_3 depletion to variations in the heat flux during the past two decades while Cl_y has been high relative to 1980 levels. The ozone value where the two lines intersect, 460 DU, represents the point where wave driving is sufficient to inhibit heterogeneous loss, and is very close to the implied climatological mean value used in WMO Figure 3.4. This analysis shows that O_3 resupply is roughly twice as sensitive to wave driving as depletion is (11.7 compared to 4.7 DU/Kms^{-1}). The attribution of an Arctic ozone increase to declining halogens will be very difficult because of the relative size of these sensitivities. Most of the difference between the observed O_3 record and 455 DU is due to the variability of resupply, not depletion. Given the slope uncertainties, depletion therefore explains about 30 (±20)% of the observed difference from 455 DU. In other words, depletion accounts for at most half, but more likely less than half of the difference from 455 DU, with the remainder of difference coming from variability in the wave-driven supply of O_3. Bednarz et al. [2016] found that ozone depletion contributed ~30% to March Arctic ozone variability in a 100-yr simulation with the UM-UKCA chemistry climate model, concluding as we do that dynamical variability is the primary contributor to interannual variations in Arctic spring column O_3.

Tegtmeier et al. [2008] performed a similar analysis to determine dynamical supply and depletion sensitivities to wave driving from December to mid-March, 1992-2004. They concluded that inside the vortex those sensitivities were the same. Their method to estimate the dynamical contribution to polar O_3 explicitly neglected meridional mixing into the vortex as well as column O_3 changes above 550 K (30

hPa). Their depletion was calculated with the Match method using O_3 sondes and a trajectory model [Rex et al., 2006]. As discussed in Livesey et al. [2015a], meridional transport and mixing add uncertainty to the Match calculation of vortex-averaged chemical loss. Although we find similar year-to-year loss variability, our results differ from Tegtmeier et al. [2008] in part because we are calculating the March mean total column O_3 63-90°N, which includes some non-vortex air, rather than a vortex-averaged quantity. But differences are also likely because our method accounts for rather than neglects O_3 changes due to transport and mixing.

5. The Net Effect of Dynamics and Depletion on April O_3

This study has two key findings that are relevant to understanding midlatitude spring O_3 variability. First, most of the interannual variability in the Arctic March mean O_3 comes from resupply variability rather than depletion. And second, the seasonal ozone depletion in years with a cold, stable vortex is on average 3 times greater and occurs one month later (March) than disturbed years. In this section we examine the effects of these findings in April and consider the spatial variations of their effects on midlatitude O_3 and surface UV index (UVI) variability. We calculate the MLS total column O_3 by combining MLS stratospheric column O_3 with the GMI tropospheric O_3 column. We also calculate a 'No Het Loss' MLS O_3 column by adding GMI-calculated depletion to the MLS total column.

Figure 9 looks at differences in the effects of depletion (top row) and resupply (bottom row) to the April mean total column O_3 north of 20°N after cold and warm winters. Figures 9a and 9b show the net change due only to depletion in cold and warm years, and Fig. 9c shows the difference between them. The Aprils that follow a cold winter have 10-20 DU greater depletion over northern Europe and Asia (0-130°E) and up to ~5 DU greater depletion over North America (near 250°E) than those following warm winters; the white boxes on panels c and g indicate the European and North American regions. Panels in the bottom row, Figs. 9e-h, are calculated with the MLS 'No Het Loss' column O_3. Figs. 9e and 9f show the April total column O_3 distributions after warm and cold winters; Fig. 9g shows the mean differences between them, due only to dynamics. There is large longitudinal variability. Dynamics contributes up to 18 DU more and up to 30 DU less O_3 at certain longitudes between 50-70°N after cold winters. This is often larger than the depletion differences in Fig. 9c (directly above Fig. 9g).

Figures 9c (depletion) and 9g (dynamics) show the different causes of column O_3 variability after cold and warm winters. Their net effect varies strongly with region. Consider the boxes drawn on these panels, representing the locations of many ground-based measurements stations in Europe (longitudes 0-30°E) and North America (longitudes 235-290°E). Over Europe the net effect in April after cold years is

8-18 DU lower O_3 than in warm years, with similar contributions from depletion and dynamics. But over North America, while there is some O_3 depletion (Fig. 9c) there is a greater increase in O_3 supply (Fig. 9g), with the net effect that O_3 is up to 10 DU higher after cold years. Ground-based column O_3 measurements from Europe and North America will show different April variability due to longitudinal variations in O_3 transport and the export of polar O_3 depletion.

To assess the significance of Arctic ozone loss on surface UV, we calculate the clear sky impact on the surface UV index from the O_3 changes shown in Fig. 9c and 9g using a lookup table of UVI as a function of overhead ozone and solar zenith angle [Newman and McKenzie, 2011]. The right-hand side panels (Figs. 9d and 9h) show how depletion and dynamics affect the April UVI differently after cold and warm winters. Typical April mean clear sky UV indices range from 10 at 30^{o}N to 3 at 60^{o}N (not shown). Depletion has small impacts on UVI in April, 0.1-0.2 after cold winters and 0-0.1 after warm winters; the difference in their impact is 0-0.1 (Fig. 9d). Although there are large differences in depletion after warm and cold winters (Figs. 9a and 9b), the impact on UVI at polar latitudes is negligible due to low solar zenith angles in early spring. In the midlatitudes, sun angles are higher but the depletions are <10 DU in both cold and warm winters, thus the impact of depletion on UVI is small here too, <0.2. However, the cold-warm dynamical differences in the midlatitudes are much larger than depletion differences (Fig. 9h). They show a larger increase in surface UVI, up to 0.3 over Asia (70-130^{o}E), but a lower UVI over North American longitudes after cold Arctic winters. Overall the effects of Arctic ozone depletion on April surface UVI are small. The primary source of clear sky April UVI variability in the mid and high latitudes is column O_3 dynamical variability.

6. Summary and Conclusions

We used realistic simulations from the GMI CTM with and without heterogeneous halogen chemistry to quantify the heterogeneous chemical loss and the dynamical contributions to March Arctic ozone for the winters 2005-2015. We found that the maximum Arctic O_3 loss each season, averaged over 63-90^o equivalent latitude, depends linearly on the number of days that lower stratospheric vortex temperatures were below the threshold for halogen activation on PSC particles. The occurrence of a stratospheric sudden warming strongly influences the number of cold days in the vortex. Winters with a major SSW had the fewest cold days and the least O_3 loss, while years with no major or minor warming before mid-February had the most cold days and the greatest O_3 loss. From 2005-2015, 5 years had weak wave activity and a persistently cold vortex. The average O_3 loss in those years was nearly 3 times greater than years with a minor or major SSW, and the areal extent of the loss was also greater. The

463 maximum O_3 loss in cold years occurred in mid-March, approximately 1 month later than the warmer
464 years. All of these factors led to greater export of ozone depleted air to the midlatitudes in years with a
465 cold and weakly disturbed polar vortex. Aprils following a disturbed winter vortex have 2-8 DU
466 depletions between 30°-60°N while Aprils following a cold vortex have an average depletion of 5-15 DU.
467 Even after cold winters, depletion has a very small impact on surface UVI in April, causing on average
468 less than a 0.2 increase in surface UV index at any latitude, and generally less than 0.1.

469 Dynamically-driven (i.e., transport) differences in the O_3 distribution between warm and cold Arctic
470 winters have a much larger effect on mid and high latitude spring O_3 than does the export of polar
471 depletion. Some longitudes will have lower O_3 after cold winters due to a combination of depletion and
472 dynamics, while other longitudes will have higher O_3 because a positive dynamical contribution
473 dominates a small depletion. Trends calculated from ground-based column O_3 measurements in the
474 northern mid and high latitudes may be affected by the large longitudinal variations in the sources of O_3
475 variability. Observed variability at European and North American sites will reflect different contributions
476 from ozone-depleted air and from transport, with neither location representative of the zonal mean.

477 The quantitative relationship identified between cold days and ozone depletion during the Aura period
478 made it possible to estimate Arctic spring ozone loss from 1993-2004 using MERRA temperatures. With
479 these estimated O_3 depletions, we produced a record of Arctic March 'No Het Loss' total column O_3 for
480 1993-2015 averaged over 63-90°N geographic latitude, the same averaging used in the WMO
481 Assessment. Each year the March observed O_3 and 'No Het Loss' O_3 vary, but the difference in their
482 sensitivities to wave driving revealed the sensitivity of depletion, independent of resupply. For every 2
483 DU that wave driving increases resupply there is about a 1 DU decrease in depletion. From 1993-2015,
484 dynamical contributions to March ozone varied by 80 DU while chemical depletion reduced O_3 between
485 1 and 39 DU. The largest depletion of this period, 10%, occurred in 2011 when the March mean loss was
486 39 DU while weak resupply reduced the 'No Het Loss' O_3 to 379 DU. Although our results are consistent
487 with previous estimates of the contributions of depletion and resupply to Arctic O_3 (Tegtmeier et al.,
488 [2008]; Chipperfield and Pyle [1999]), they represent an improvement because our methods better
489 account for vortex O_3 changes due to transport.

490 Our results explain the variability in the WMO Arctic O_3 record. Because wave driving controls both the
491 O_3 resupply (via transport) and O_3 depletion (via temperature), winters with weak wave driving (smaller
492 resupply) will have a colder, more stable vortex with greater heterogeneous ozone depletion compared
493 to winters with stronger wave activity. The 455 DU climatological March mean suggested by Figure 3.4

of WMO [Dameris and Godin-Beekmann, 2014] masks the importance of dynamical variability in determining Arctic spring O_3 each year; it is at the high end of the 375-464 DU range we find for 1993-2015 ('No Het Loss' O_3). In the future when anthropogenic ODSs are significantly lower than today, interannual variability in wave driving will continue to produce large variability in Arctic March O_3.

Using the relationship found in this study between cold days and ozone depletion, we estimate that the Arctic winter of 2016 had a 63-90°N EqL seasonal maximum O_3 depletion of about 40 DU. MERRA shows that the low temperatures required for depletion persisted in the 2015/2016 Arctic vortex for 84 days, about the same as 2005 and 2014. The winter of 2011 had 105 days (3.5 months) with temperatures low enough for chlorine activation, the most in the 1993-2015 record examined here.

With inorganic chlorine levels declining, it is unlikely that future Arctic winters will exceed the 2011 ozone loss, however, the decadal scale impact of depletion could increase. From 2005-2015, the mean maximum Arctic cap ozone depletion for equivalent latitudes 63-90°N was 28 DU and it was modulated by the frequency of SSWs: 6 of 11 recent winters had a major or minor warming before mid-February that kept depletion below 22 DU. This frequency is similar to that reported by Charlton and Polvani [2007] based on 40 years of reanalyses. Within that 40-year period they found large decadal scale variability in SSW frequency, with an SSW in every year of the 1980s but only 2 in the 1990s. In spite of the projected decline in polar stratospheric Cl_y levels of ~22 ppt/yr [Strahan et al., 2014], Cl_y levels during the next two decades will remain above 2 ppb, enough to cause significant ozone depletion. If the coming decades experience a reduced frequency of SSWs similar to the 1990s, Arctic ozone depletion may appear to become a more serious problem in spite of declining chlorine levels. The improved understanding of the role of dynamics in winter and spring O_3 distributions gained in this study will allow a more accurate attribution of sources of O_3 variability in future observations.

Acknowledgments. This work was supported by the NASA Modeling, Analysis, and Prediction Program and the NASA Atmospheric Composition Modeling and Analysis Program. MLS data are available at http://mls.jpl.nasa.gov. The MERRA reanalysis can be obtained from the Goddard Earth Science Data and Information Services Center, http://disc.sci.gsfc.nasa.gov/daac-bin/DataHoldings.pl. Derived meteorological quantities such as heat fluxes can be obtained through this NASA data services website (http://acdb-ext.gsfc.nasa.gov/Data_services/met/ann_data.html). GMI simulation output is available by request to susan.e.strahan@nasa.gov. We thank the reviewers for their constructive comments.

Appendix - Evaluation of the GMI-MERRA simulation

Arctic ozone changes during winter are a result of a dynamical (transport) contribution and heterogeneous chemical loss. Both must be realistically represented in order to accurately simulate ozone. We demonstrate the fidelity of the GMI simulation with full chemistry by comparing it with Aura MLS O_3 and N_2O observations. The N_2O comparison is used to evaluate lower stratospheric transport independent of polar ozone chemistry. N_2O changes during winter, averaged over the Arctic cap (63-90^{o}N equivalent latitude), are driven by diabatic descent and meridional mixing. If winter transport is realistic, then the Arctic ozone comparison gauges how well chemical loss is well represented.

Figure A1 compares the evolution of Arctic cap average N_2O (450 K) and stratospheric column O_3 for MLS and GMI during winter and spring in 4 years. Each species is plotted as the change with respect to its Arctic cap value averaged over 1-10 December. The years were chosen to show the CTM performance under a wide range of dynamical conditions during the Aura period; they are ordered left to right by the day of the final warming. 2013 had an early January major SSW, 2010 had a mid-February minor SSW, 2005 had a large cold vortex with a March final warming, and 2008 had a small cold vortex with an April final warming. The onset of vortex breakdown is shown by the dashed red line. This was determined by the date when the equivalent latitude of the 450 K vortex edge reached or exceeded 75^o, resulting in an area of less than 1/3 of the 63-90^o polar cap (< 9 million km^2). The dashed blue line is 3 days after the final date of temperatures below the chlorine activation threshold, chosen to represent the point when nearly all ozone depletion has ceased. The top row of Figure A1 shows that the seasonal change in GMI N_2O (black) tracks closely with observed changes (red) throughout the winter, indicating a good representation of vortex isolation and descent. Poorer agreement is found after a SSW and after the final warming when mixing with midlatitude air occurs. However, the period of ozone depletion (dates to the left of blue dashed line) show excellent transport fidelity, suggesting that dynamical changes to O_3 that occur during depletion are well-represented. Good agreement between vortex GMI and MLS O_3, N_2O, and ClO is also found in the very cold winter of 2011. This was shown in Strahan et al. [2013] and is not repeated here.

The bottom row of Figure A1 shows excellent agreement in all 4 years between MLS and GMI Arctic cap stratospheric column O_3 during the period of ozone depletion. Because transport is well-represented during this period, the excellent agreement between MLS and GMI column O_3 indicates that the chemical loss is also well represented. For the 2005-2015 period, the average difference between MLS and GMI O_3 change during the depletion period is 1 DU with a standard deviation of 8 DU. GMI

555 stratospheric column O_3 also has very good agreement with MLS through the end of March. The average
556 December to March Arctic O_3 change is 77 DU for both MLS and GMI, and one standard deviation of the
557 GMI O_3 error is 8 DU, about 10%. The ability of the simulated column O_3 and lower stratospheric N_2O to
558 closely track the MLS observed changes during winter demonstrates that this simulation is well-suited
559 for the calculation of heterogeneous chemical loss and dynamical contributions to Arctic ozone.

560

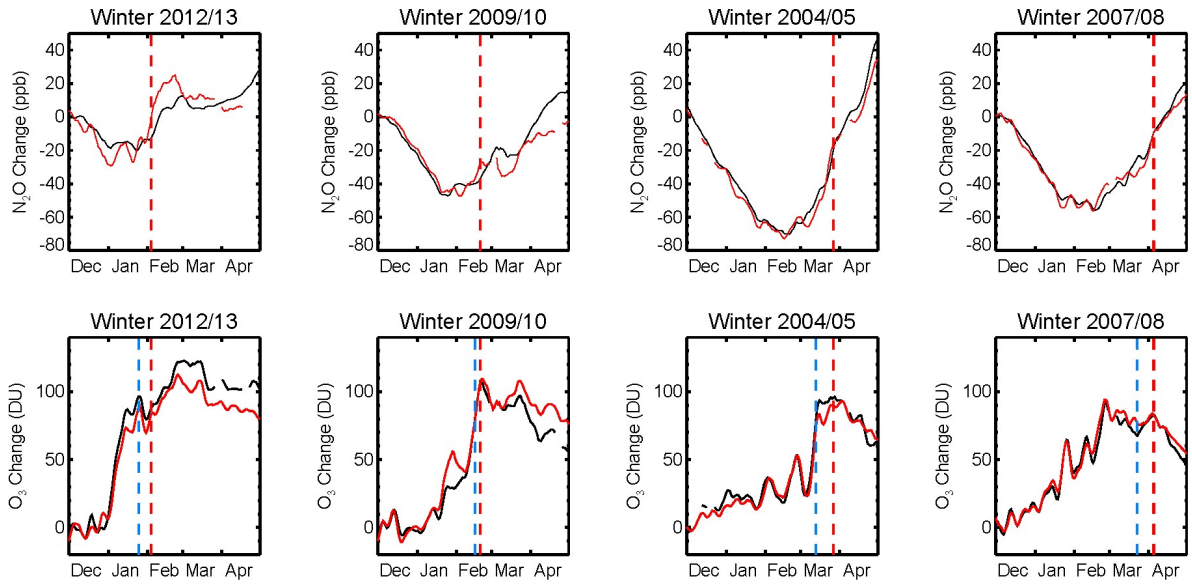

561

562 Figure A1. Evaluation of GMI performance in the Arctic during 4 dynamically different winters. All
563 panels compare the seasonal evolution of the Arctic cap (63-90°N EqL) average of GMI (black) and MLS
564 (red) trace gases relative to their value averaged from December 1-10. Top panels show N_2O change (in
565 ppb) on the 450 K surface. Bottom panels show stratospheric column O_3 change (DU). The red dashed
566 line indicates the date of the final warming, which ranges from early February to early April in the 4
567 years. The blue dashed line falls 3 days after the final date of temperatures below the chlorine activation
568 threshold in the lower stratosphere.

References

Abalos, M., B. Legras, F. Ploeger, and W.J. Randel (2015), Evaluating the advective Brewer-Dobson circulation in three reanalyses for the period 1979-2012, J. Geophys. Res., 120, doi:10.1002/2015JD023182.

Andrews, D.G., J.R. Holton, and C.B. Leovy (1987), Middle atmosphere dynamics, Academic Press, Inc., London.

Bednarz, E.M., A.C. Maycock, N.L. Abraham, P. Braesicke, O. Dessens, and J.A. Pyle (2016), Future Arctic ozone recovery: the importance of chemistry and dynamics, Atmos. Chem. Phys. Disc., doi:10.5194/acp-2015-998.

Charlton, A.J. and L.M. Polvani (2007), A new look at stratospheric sudden warmings: Part I: Climatology and modeling benchmarks, J. Climate, 20, 449-469.

Chipperfield, M.P. and R.L. Jones (1999), Relative influences of atmospheric chemistry and transport on Arctic ozone trends, Nature, 400, 551-554.

Dameris, M. and S. Godin-Beekmann (2014), Update on global ozone: Past, present, and future, Chapter 3 in Scientific Assessment of Ozone Depletion: 2014, Global Ozone Research and Monitoring Project – Report No. 55, World Meteorological Organization, Geneva, Switzerland.

Hanson, D. and K. Mauersberger (1988), Laboratory studies of the nitric acid trihydrate: Implications for the south polar stratosphere, Geophys. Res. Lett., 15, 855-858.

Kawa, S. R., et al. (1997), Activation of chlorine in sulfate aerosol as inferred from aircraft observations, J. Geophys. Res., 102, 3921-3933.

Kuttipurrath, J. and G. Nikulin (2012), A comparative study of the major sudden stratospheric warmings in the Arctic winters 2003/2004-2009/2010, Atmos. Chem. Phys., 12, 8115-8129.

Lawrence, Z.D., G.L. Manney, K. Minschwaner, M.L. Santee, and A. Lambert (2015), Comparisons of polar processing diagnostics from 34 years of the ERA-Interim and MERRA reanalyses, Atmos. Chem. Phys., 15, 3873-3892.

Li, F., D.W. Waugh, A.R. Douglass, P.A. Newman, S. Pawson, R.S. Stolarski, S.E. Strahan, and J.E. Nielsen (2012), Seasonal variations of stratospheric age spectra in the Goddard Earth Observing System Chemistry Climate Model (GEOSCCM), J. Geophys. Res., 117, D05134, doi:10.1029/2011JD016877.

Livesey, N., et al. (2011), Earth Observing System (EOS) Aura Microwave Limb Sounder (MLS) Version 3.3 Level 2 data quality and description document, JPL D-33509.

599 Livesey, N.J., M.L. Santee, and G.L. Manney (2015a), A Match-based approach to the estimation of polar
600 stratospheric ozone loss using Aura Microwave Limb Sounder observations, Atmos. Chem. Phys.,
601 15, 9945–9963.
602 Livesey, N.J., et al. (2015b), Earth Observing System (EOS) Aura Microwave Limb Sounder (MLS) Version
603 4.2x Level 2 data quality and description document, JPL D-33509 Rev. A.
604 Manney, G.L., L. Froidevaux, M.L. Santee, N.J. Livesey, J.L. Sabutis, and J.W. Waters (2003), Variability of
605 ozone loss during Arctic winter (1991–2000) estimated from UARS Microwave Limb Sounder
606 measurements, J. Geophys. Res., 108, 4149, doi:10.1029/2002JD002634.
607 Manney, G.L., Z.D. Lawrence, M.L. Santee, N.J. Livesey, A. Lambert, and M.C. Pitts (2015), Polar
608 processing in a split vortex: Arctic ozone loss in early winter 2012/2013, Atmos. Chem. Phys., 15,
609 5381-5403.
610 Mueller, R., U. Schmidt, A. Engel, D.S. McKenna, and M.H. Proffitt (2001), The O_3-N_2O relation from
611 balloon-borne observations as a measure of Arctic ozone loss in 1991/92, Q.J.R. Meteorol. Soc.,
612 127, 1389-1412.
613 Mueller, R., S. Tilmes, P. Konopka, J.-U. Groos, and H.-J. Jost (2005), Impact of mixing and chemical
614 change on ozone-tracer relations in the polar vortex, Atmos. Chem. Phys., 5, 3139-3151.
615 Mueller, R., J.-U. Grooss, C. Lemmen, D. Heinze, M. Dameris, and G. Bodeker (2008), Simple measures of
616 ozone depletion in the polar stratosphere, Atmos. Chem. Phys., 8, 251-264.
617 Nash, E.R., P.A. Newman, J.E. Rosenfield, and M.R. Schoeberl (1996), An objective determination of the
618 polar vortex using Ertel's potential vorticity, J. Geophys. Res., 101, 9471-9478.
619 Newman, P.A., E. R. Nash, and J. E. Rosenfield (2001), What controls the temperature of the Arctic
620 stratosphere during the spring?, J. Geophys. Res., 106, D17, doi:10.1029/2000JD000061.
621 Newman, P.A., S.R. Kawa, and E.R. Nash (2004), On the size of the Antarctic ozone hole, Geophys. Res.
622 Lett., 31, L21104, doi:10.1029/2004GL020596.
623 Newman, P.A., E.R. Nash, S.R. Kawa, S.A. Montzka, and S. Schauffler (2006), When will the Antarctic
624 ozone hole recover?, Geophys. Res. Lett., 33, L12814, doi:10.1029/2005GL025232.
625 Newman, P.A., J.S. Daniel, D.W. Waugh, and E.R. Nash (2007), A new formulation of equivalent effective
626 stratospheric chlorine (EESC), Atmos. Chem. Phys., 7, 4537-4552.
627 Newman, P.A. and R. McKenzie (2011), UV impacts avoided by the Montreal Protocol, Photochem.
628 Photobiol. Sci., 2011, 10, 1152–1160.

629 Randel, W.J., F. Wu, and R. Stolarski (2002), Changes in column ozone correlated with the stratospheric
630 EP flux, J. Met. Soc. Jap., 80, 849-862.
631 Rex, M., et al. (2002), Chemical depletion of Arctic ozone in the winter 1999/2000, J. Geophys. Res., 107,
632 8276, doi:10.1029/2001JD000533.
633 Rex, M., R.J. Salawitch, P. von der Gathen, N.R.P. Harris, M.P. Chipperfield, and B. Naujokat (2004), Arctic
634 ozone loss and climate change, Geophys. Res. Lett, 31, doi:10.1029/2003GL018844.
635 Rex, M., et al. (2006), Arctic winter 2005: Implications for stratospheric ozone loss and climate change,
636 Geophys. Res. Lett., 33, L23808, doi:10.1029/2006GL026731.
637 Rienecker, M.M. et al. (2011), MERRA: NASA's Modern Era Retrospective Analysis for Research and
638 Applications, J. Climate, 24, 3624-3648.
639 Schoeberl, M.R., A.R. Douglass, Z. Zhu, and S. Pawson (2003), A comparison of the lower stratospheric
640 age spectra derived from a general circulation model and two data assimilation systems, J.
641 Geophys. Res., 108, doi:10.1029/2002JD002652.
642 Strahan, S. E., A.R. Douglass, and P.A. Newman (2013), The contributions of chemistry and transport to
643 low Arctic ozone in March 2011 derived from Aura MLS observations, J. Geophys. Res., 118, 1563–
644 1576, doi:10.1002/jgrd.50181.
645 Strahan, S.E., A.R. Douglass, P.A. Newman, and S.D. Steenrod (2014), Inorganic chlorine variability in the
646 Antarctic vortex and implications for ozone recovery, J. Geophys. Res., 119,
647 doi:10.1002/2014JD022295.
648 Tan, W.W., M.A. Geller, S. Pawson, and A. DaSilva (2004), A case study of excessive subtropical transport
649 in the stratosphere of a data assimilation system, J. Geophys. Res., 109, D11102,
650 doi:10.1029/2003JD004057.
651 Tegtmeier, S., M. Rex, I. Wohltmann, and K. Krueger (2008), Relative importance of dynamical and
652 chemical contributions to Arctic wintertime ozone, Geophys. Res. Lett., 35, L17801,
653 doi:10.1029/2008GL034250.
654 Tilmes, S., R. Mueller, J.-U. Grooss, D.S. McKenna, J.M. Russell III, and Y. Sasano (2003), Calculation of
655 chemical ozone loss in the Arctic winter 1996–1997 using ozone-tracer correlations: Comparison of
656 Improved Limb Atmospheric Spectrometer (ILAS) and Halogen Occultation Experiment (HALOE)
657 results, J. Geophys. Res., 108, 4045, doi:10.1029/2002JD002213.
658 Weber, M., S. Dhomse, F. Wittrock, A. Richter, B.-M. Sinnhuber, and J.P. Burrows (2003), Dynamical
659 control of NH and SH winter/spring total ozone from GOME observations in 1995-2002, Geophys.
660 Res. Lett., 30, 1583, doi:10.1029/2002GL016799.

Weber, M., S. Dikty, J.P. Burrows, H. Garny, M. Dameris, A. Kubin, J. Abalichin, and U. Langematz (2011), The Brewer-Dobson circulation and total ozone from seasonal to decadal time scales, Atmos. Chem. Phys., 11, 11221-11235.

Wohltmann, I., et al. (2013), Uncertainties in modelling heterogeneous chemistry and Arctic ozone depletion in the winter 2009/2010, Atmos. Chem. Phys., 13, 3909-3929.

WMO (World Meteorological Organization) (2014), Scientific Assessment of Ozone Depletion: 2014, Global Ozone Research and Monitoring Project – Report No. 55, 416 pp., Geneva, Switzerland.

669

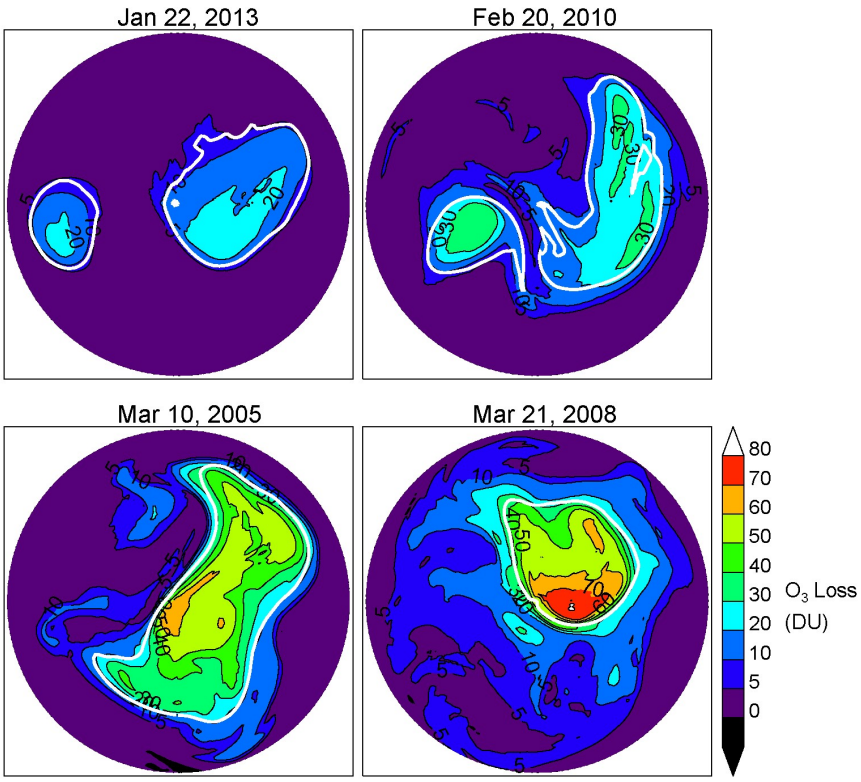

670

671 Figure 1. Total column heterogeneous chemical ozone loss in Dobson units calculated from GMI
672 simulations in 4 dynamically different years. The top panels show dynamically disturbed years while the
673 bottom panels show dynamically quiet years with a longer-lived vortex. Each date chosen shows Arctic
674 ozone depletion near its seasonal maximum for that year. The white contour indicates the edge of the
675 450 K polar vortex as defined by the region of maximum potential vorticity gradients [Nash et al., 1996].

676

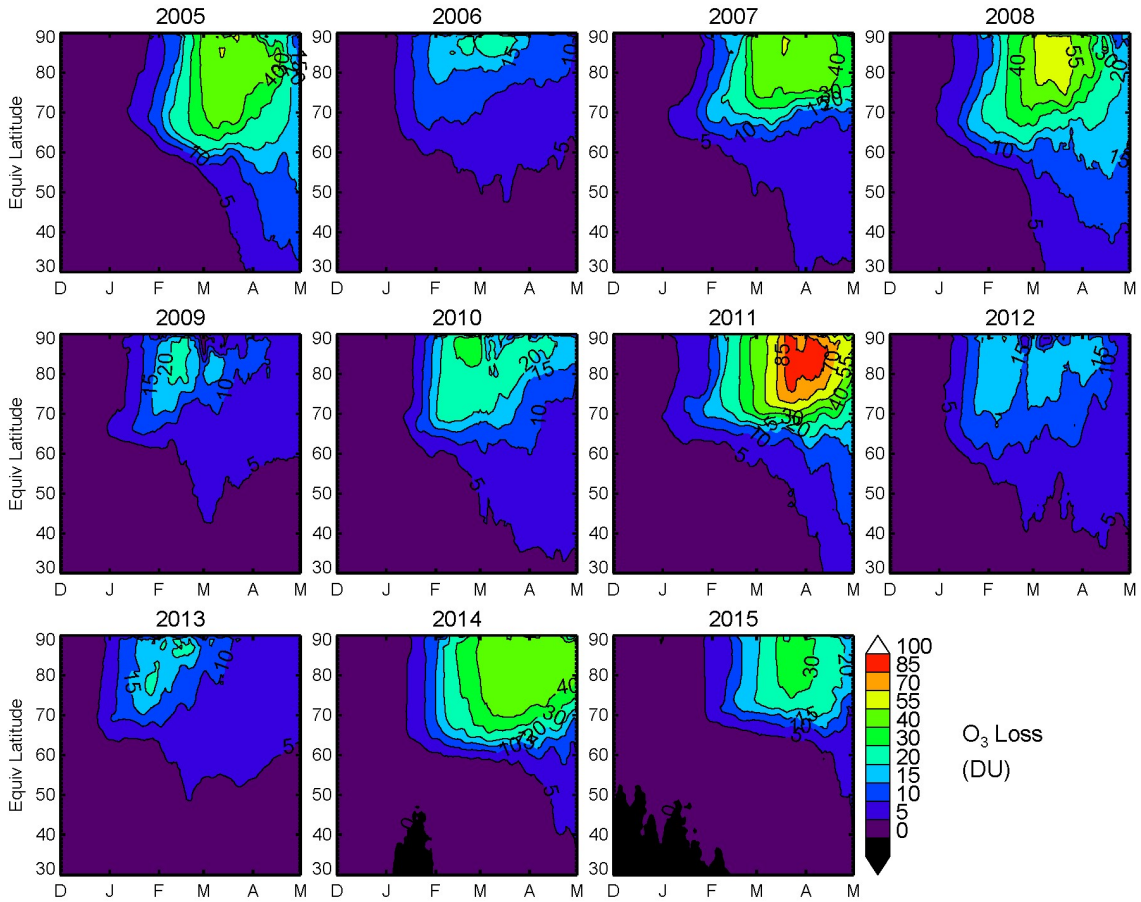

677

678 Figure 2. Daily total column heterogeneous chemical ozone loss (DU) from the GMI simulations,
679 December to May for all years 2005-2015 as a function of equivalent latitude. The years with losses >40
680 DU have a much larger impact on the midlatitudes in spring.

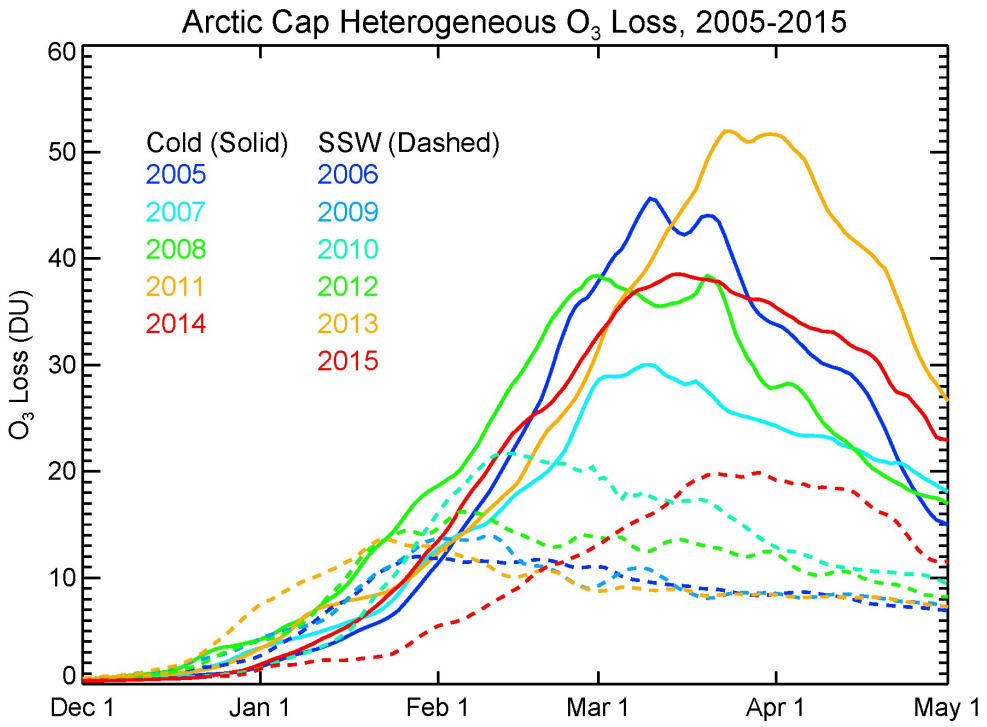

681

682 Figure 3. Time series of Arctic cap average (63-90°N EqL) heterogeneous chemical O_3 losses for 11 years.

683 The results shown used 5-day smoothing.

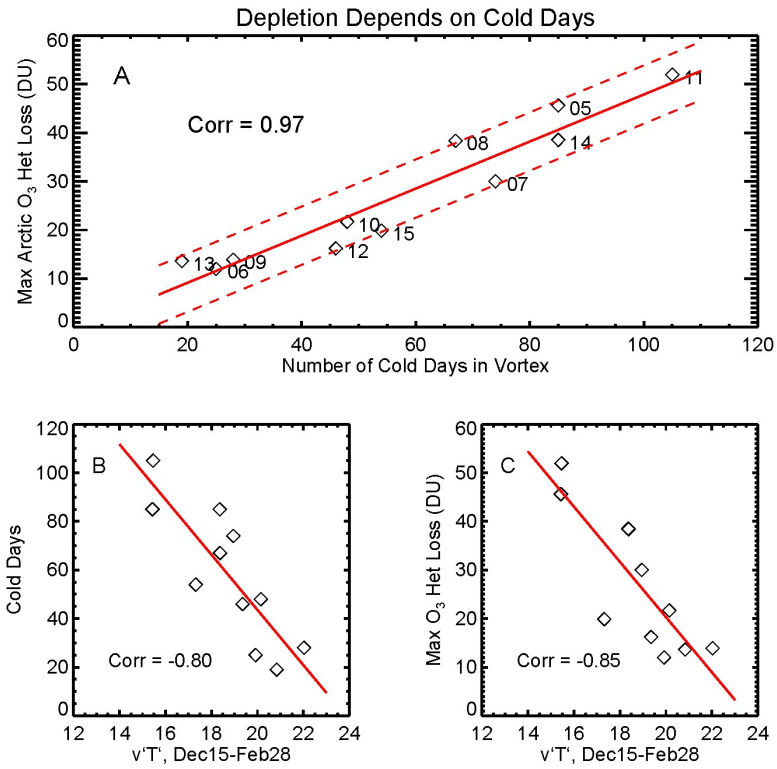

684

685 Figure 4. a) The linear relationship between the maximum Arctic cap column ozone depletion and the
686 number of cold days in the Arctic lower stratospheric vortex. The correlation of the 11 points is 0.97. The
687 dashed lines are ±6 DU of the fitted line. The number of cold days b) and the maximum ozone
688 heterogeneous loss c) are both significantly correlated with wave driving (the 45-75^{o}N zonal mean 100
689 hPa heat flux, v'T', in units of Kms^{-1}) averaged over Dec 15-Feb 28.

690

691

692

693

694

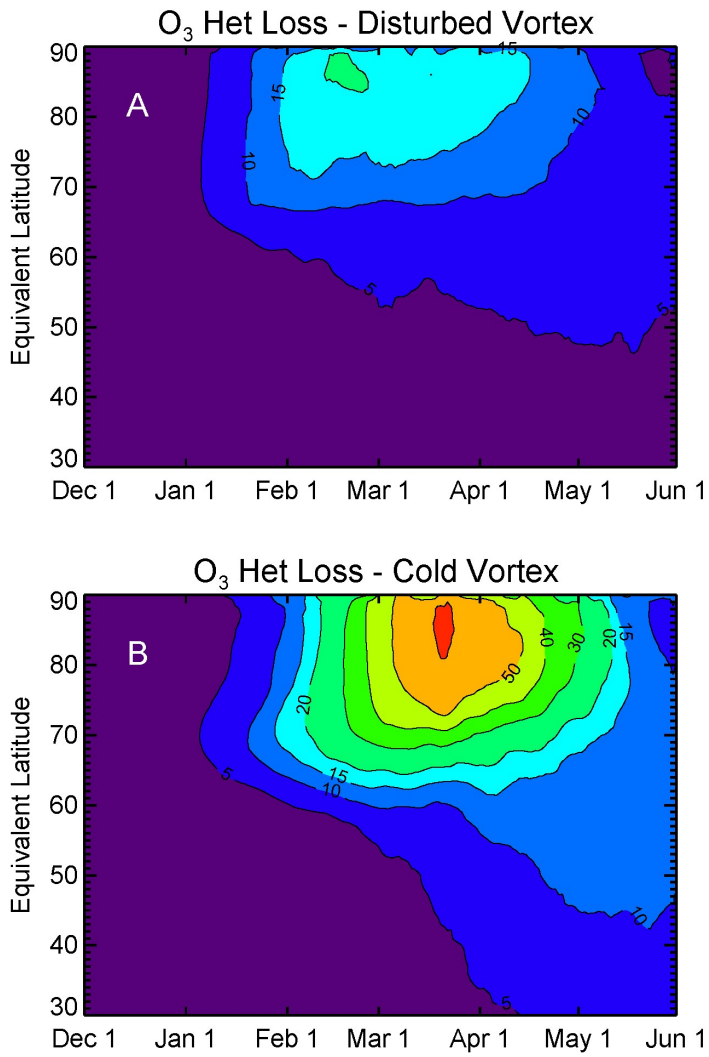

695

696 Figure 5. The average column ozone depletion (DU) for a) 6 years with SSWs and b) 5 years with no
697 major or minor SSW before mid-February. The maximum depletion in years without a midwinter
698 warming is roughly 3 times greater than years with a warming.

699

700

701

702

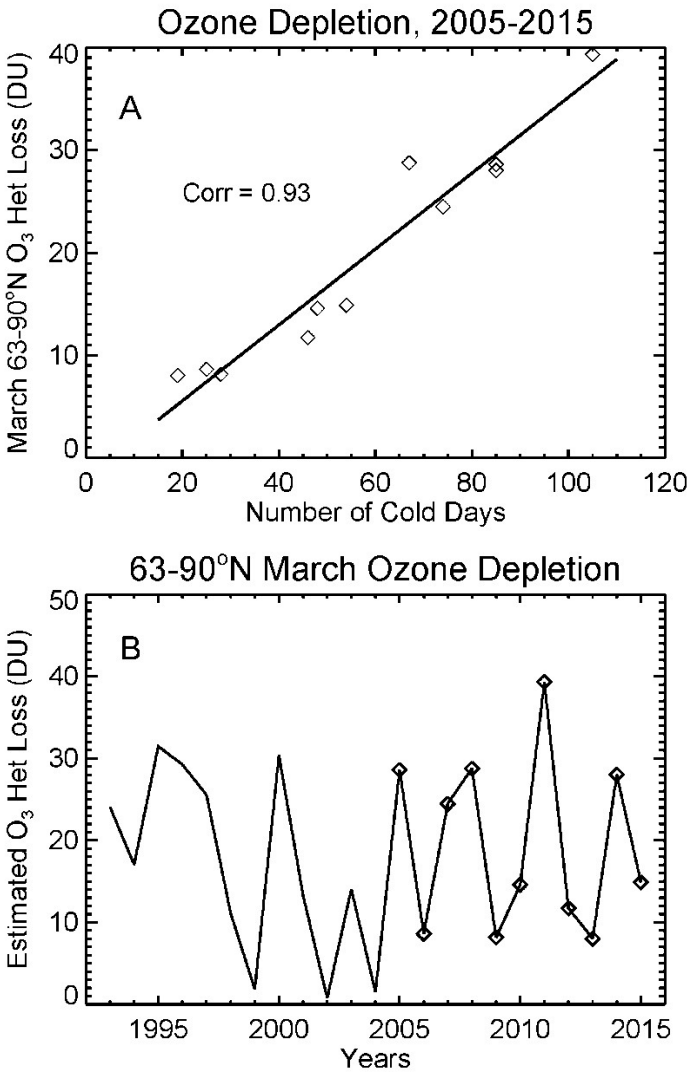

703

704 Figure 6. a) The relationship between the number of cold days each winter and the March average
705 ozone depletion (DU) average over the geographic pole, 63-90°N. This is the basis for estimating O_3
706 depletion for years prior to the Aura period. b) The estimated geographic polar cap March average
707 depletion (DU) for years 1993-2004 calculated with the slope of the fitted line in a) and the number of
708 cold days determined from the MERRA reanalysis. Polar cap loss for 2005-2015 (diamonds) was
709 calculated with the GMI simulations (i.e., the points in panel a)).

710

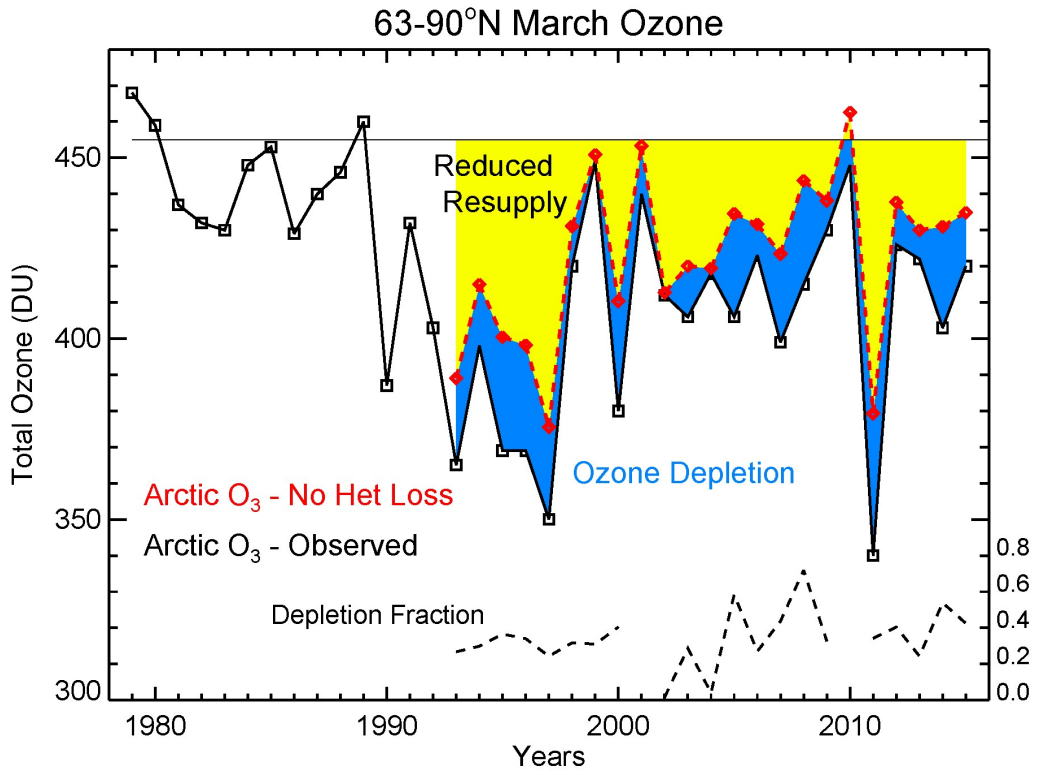

711

712 Figure 7. The 63-90°N March average total column O_3 from satellite observations, 1979-2015 (black).
713 The red dashed line shows the 'No Het Loss' O_3, calculated as the sum of the observed column O_3 and
714 the loss estimates in Fig. 6b. The amount of loss each year is shown by blue shading. The thin line at 455
715 DU comes from the WMO [2014] figure and represents their assumed climatological mean value for
716 March O_3. The difference between the 'No Het Loss' O_3 and 455 DU (yellow shading) shows the impact
717 of wave driving on resupply. The amount of depletion (blue) with respect to the observations' difference
718 from 455 DU (yellow+blue) is shown as a dashed line near the bottom.

719

720

721

722

723

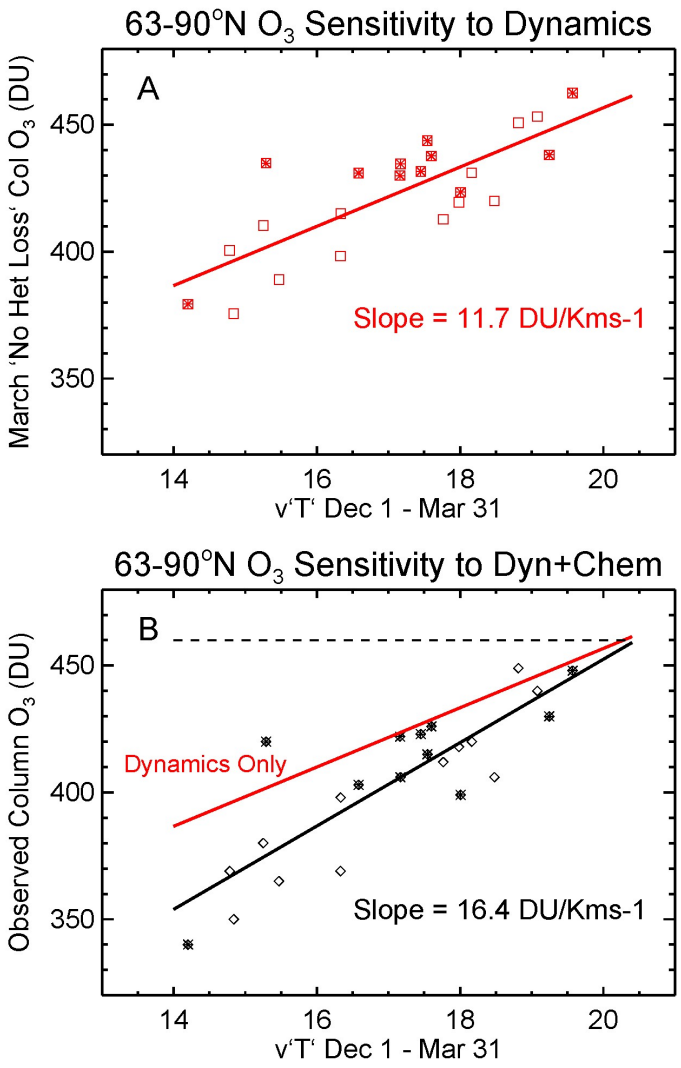

724

725 Figure 8. a) The relationship between March mean 'No Het Loss' column O_3 (DU), 63-90°N, and the
726 mean heat flux (Kms^{-1}) averaged Dec 1-Mar 31, the period when wave driving influences March O_3. The
727 slope of the best fit line (red) quantifies the sensitivity of polar O_3 resupply to wave driving. b) The
728 relationship between observed March mean column O_3 and the mean heat fluxes (black). The slope of
729 this line shows the combined sensitivities of O_3 resupply and chemical loss to wave driving. The
730 dynamics-only line from panel a) is shown in red. The intersection of these lines near 460 DU represents
731 the point where wave driving is sufficient to inhibit heterogeneous loss. For both panels, open symbols
732 are 1993-2004, filled symbols are 2005-2015.

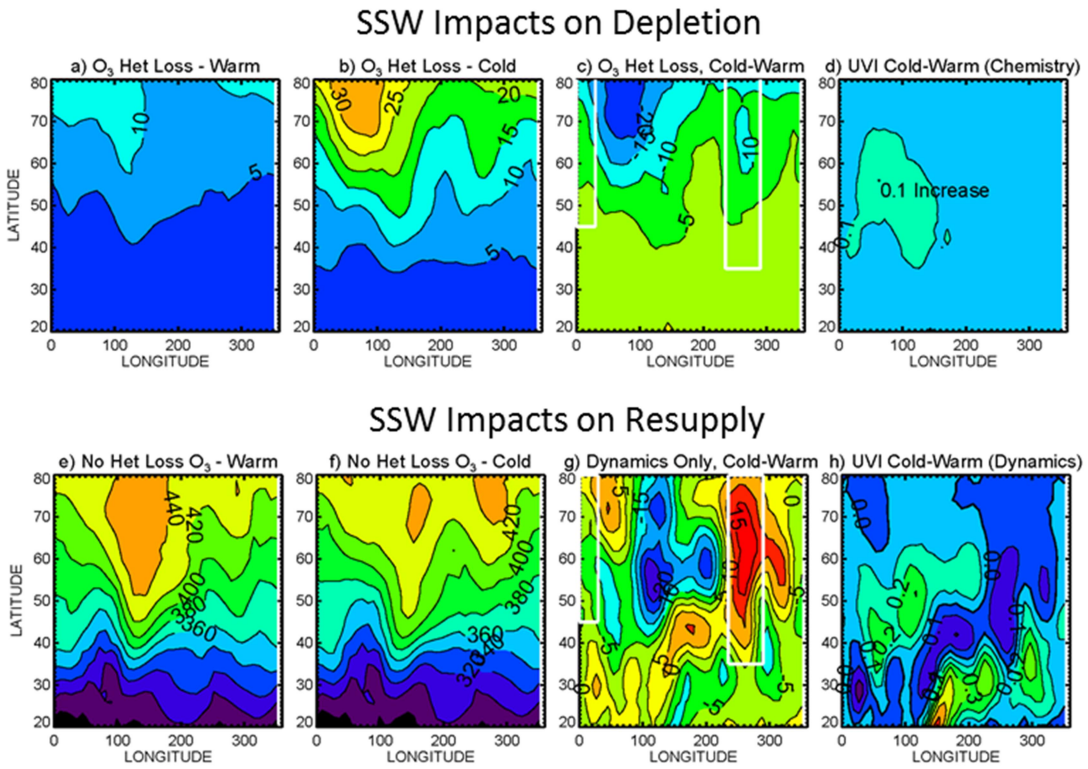

733

734 Figure 9. Separation of the effects of depletion and dynamics on April mean column O_3 after cold and
735 warm winters 20-80°N latitude, 0-360°E longitude. Panels a)-c) show mean depletions after warm and
736 cold Arctic winters, and their difference, calculated from the GMI simulations with and without
737 depletion. Panels e)-g) show warm and cold winters' dynamical effects, and their differences, using the
738 MLS 'No Het Loss' total column O_3 (see text) in order to identify the impact on O_3 distributions. Panels d)
739 and h) show the difference in impacts of depletion (d) and dynamics (h) on UV index after cold and
740 warm winters. The April mean clear sky UVI ranges from 10 at 30°N, 3 at 60°N, and 1-3 in the Arctic.